Nano Research

ISSN 1998-0124 CN 11-5974/O4
https://doi.org/10.1007/s12274-022-4131-y

Research Article

3D fully-enclosed triboelectric nanogenerator with bionic fish-like structure for harvesting hydrokinetic energy

Zhaoxu Jing[1,2,§], Jiacheng Zhang[1,3,§], Jianlong Wang[1,2], Mingkang Zhu[1,3], Xinxian Wang[1,2], Tinghai Cheng[1,2,4] (✉), Jianyang Zhu[1,3] (✉), and Zhong Lin Wang[1,4,5] (✉)

[1] *Beijing Institute of Nanoenergy and Nanosystems, Chinese Academy of Sciences, Beijing 101400, China*
[2] *School of Mechatronic Engineering, Changchun University of Technology, Changchun, Jilin 130012, China*
[3] *Institute of Robotics and Intelligent Systems, Wuhan University of Science and Technology, Wuhan, Hubei 430081, China*
[4] *CUSTech Institute of Technology, Wenzhou, Zhejiang 325024, China*
[5] *School of Materials Science and Engineering, Georgia Institute of Technology, Atlanta, GA 30332-0245, USA*
[§] *Zhaoxu Jing and Jiacheng Zhang contributed equally to this work.*

Received: 24 December 2021 / **Revised:** 29 December 2021 / **Accepted:** 31 December 2021

ABSTRACT

The hydrokinetic energy of river current, as one of the essential and widespread renewable energies, is difficult to be harvested in low flow velocity and shallow water areas. In this work, a three-dimensional (3D) fully-enclosed triboelectric nanogenerator (FE-TENG) with bionic fish-like structure for harvesting hydrokinetic energy is reported, which is comprised of the triboelectric power-generation unit, bionic fish-like structure and connection unit. Through the bionic structure, the FE-TENG realizes zero head power generation in shallow water with low flow velocity. What's more, the effect of external excitations and bionic structures on the electrical performance are systematically studied in this work. The FE-TENG can generate peak power density of 7 and 0.36 W/m³ respectively under the simulated swing state with frequency of 1.25 Hz and simulated river current with flow velocity of 0.81 m/s. In practical applications, due to the 3D fully-enclosed design, the FE-TENG immersed in water for 35 days demonstrates excellent immersion durability with undiminished electrical performance. Therefore, the work proposes an efficient method realizing zero head power generation, and provides a good candidate for long-term service in the river current.

KEYWORDS

hydrokinetic energy, three-dimensional (3D) fully-enclosed design, triboelectric nanogenerator, bionic fish-like structure, zero head power generation, water immersion durability

1 Introduction

With the sustainable expansion of the world economy and rapid advancement of industrialization, the demand for energy continues to increase. Therefore, developing renewable energies is required to reduce dependence on the fossil fuels [1–4]. At present, the hydro energy that occupies an important position in large-scale available energy is mainly generated from the gravitational potential energy of water stored by the dam. However, the construction of dams is severely restricted by geographical environment, and causes permanent and irreversible damage to the ecological environment [5, 6]. Therefore, harvesting the hydrokinetic energy of river current directly becomes an attractive strategy. Zero head turbine realizes power generation by harvesting kinetic energy of river current without dams, which is mainly composed of electromagnetic generators submerged under water with deep water levels and poor harvesting efficiency in the low frequency driven by the low flow velocity of river current [7, 8].

Triboelectric nanogenerator (TENG, also called Wang generator), invented by Wang's group in 2012, has been showing great prospect to convert mechanical energy into electricity [9–12]. Based on the coupling of the triboelectric effect and electrostatic induction [13–17], TENGs exhibit large potential applications in the fields of micro/nano power sources [18–21], self-powered sensing [22–27], blue energy [28–31], and high-voltage power sources [32–34]. In addition, various kinds of TENGs had been designed to harvest hydrokinetic energy, but mainly related to water wave energy [35–41]. And all these researches are difficult to harvest hydrokinetic energy of river current in low flow velocity and achieve zero head power generation in shallow water environment. The bionic design provides the effective means [42–45], i.e., the fins and body of fish can harvest hydrokinetic energy used for the balanced and coordinated movement in river current [46]. Taking advantages of the fish-like structure, it is significant to develop a bionic TENG for harvesting hydrokinetic energy of river current.

Herein, a 3D fully-enclosed triboelectric nanogenerator (FE-TENG) with bionic fish-like structure for harvesting hydrokinetic energy is proposed, which realizes zero head power generation in shallow water with low flow velocity. The FE-TENG is consisted of the bionic fish-like structure including a bionic shell and a pair of bionic fins, the triboelectric power-generation unit comprised

Address correspondence to Tinghai Cheng, chengtinghai@binn.cas.cn; Jianyang Zhu, zhujy@wust.edu.cn; Zhong Lin Wang, zhong.wang@mse.gatech.edu

of PTFE balls, copper electrodes and substrates, and the connection unit with two connectors at both ends and a spring held in the middle. In addition, finite element analysis of the FE-TENG is performed, demonstrating that the electrical performance and bionic fish-like structure are feasible. And then, the electrical performance is systematically explored under different external excitations and different flow velocities of simulated river current respectively. In practical applications, the FE-TENG shows excellent water immersion durability due to the 3D fully-enclosed design and demonstrates the ability to power the electronic devices. Therefore, the FE-TENG provides an efficient approach toward harvesting hydrokinetic energy of river current.

2 Results and discussion

2.1 Structure design and operating principle

The prospective applications of the FE-TENGs distributed in a river current to harvest hydrokinetic energy that provides power supply for electronic devices is shown in Fig. 1(a). Figure 1(b) illustrates the detailed structure of the FE-TENG, which can be divided into three parts: the triboelectric power-generation unit, bionic fish-like structure, and connection unit. The bionic fish-like structure includes a bionic shell and a pair of bionic fins, and connection unit is composed of two connectors at both ends and a spring held in the middle, which are combined to convert hydrokinetic energy of river current into regularly movement of the device required by the triboelectric power-generation unit that can be divided into the copper electrodes, PTFE balls and substrates. Copper electrodes are attached onto two sides of the substrates, with PTFE balls moving freely on it, which makes full utilization of space through stacking multi-layers substrates in parallel. Accordingly, the triboelectric power-generation unit is inlaid and sealed in the bionic shell, and converts the movement of the device into electrical output. Photographs of the FE-TENG and three different lengths of the bionic fins are presented in Figs. 1(c)(i) and 1(c)(ii) respectively.

Three operation states of the FE-TENG for half a cycle are schematically illustrated in Fig. 2(a). Under the impact of the river current, a vertical downward force F_1 is generated on the bionic fins, which drives the device to swing sideways (Fig. 2(a)(i)). And then, when the device swings to the maximum angle position, the torsion of the spring M_1 drives it to swing to the other side (Fig. 2(a)(ii)), and arrive in the consistent maximum angle position due to the action of the inertia and force F_1' (Fig. 2(a)(iii)). Detailed operating principle of the device and the force analysis of the spring are shown in Figs. S1 and S2 in the Electronic Supplementary Material (ESM) respectively.

The working mechanism of the triboelectric power-generation unit is indicated in Fig. 2(b). At first, based on electrostatic induction, the negative electrons and positive charges are obtained respectively when the PTFE balls contacte with the copper electrodes with different electronegativity [47, 48] (Fig. 2(b)(i)). When PTFE balls moving from left to right, the positive charges on the right electrode are induced by negative electrons gradually, and the current in the circuit is generated by the flow of negative electrons to the left copper electrode at the same time (Fig. 2(b)(ii)). When the PTFE balls are gathered in the right corner, positive charges are accumulated on the right copper electrode (Fig. 2(b)(iii)). Therefore, alternating current is generated as the reciprocating periodic motion of the PTFE balls. Furthermore, the electric potential distributions of the device are analyzed by the COMSOL Multiphysics software, as indicated in Fig. 2(c), verifies the feasible operation principle. And the pressure field distributions of the device are simulated with the flow velocity of 0.5 m/s as shown in Fig. S3 in the ESM.

2.2 Output performance

A swing apparatus is shown in Fig. 3(a), which is used to simulate

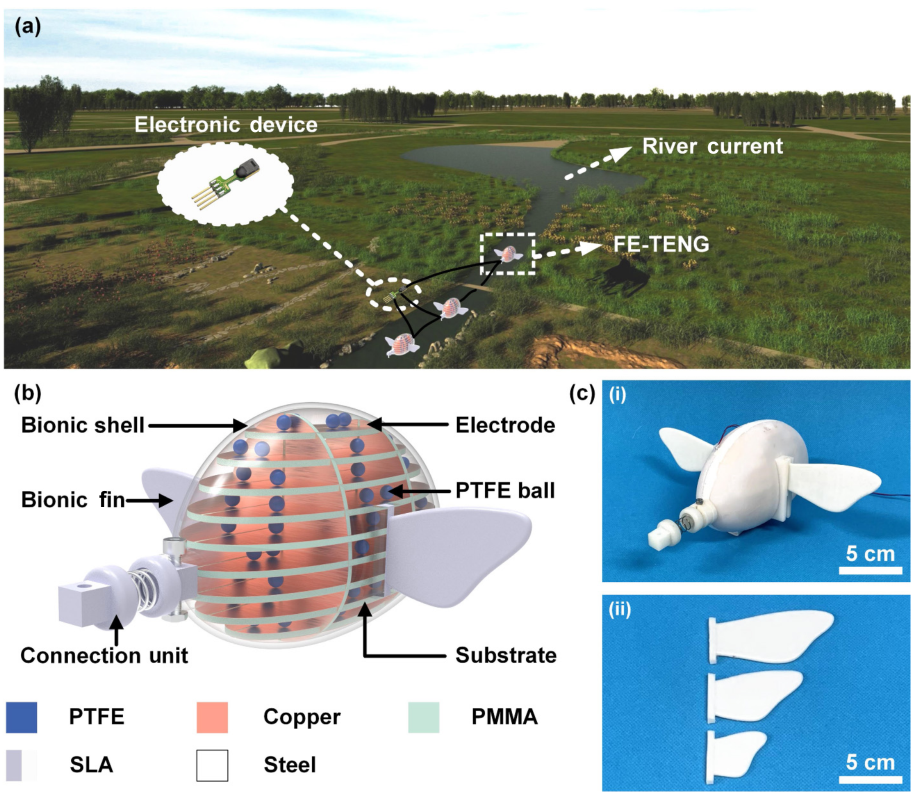

Figure 1 Schematic of the 3D fully-enclosed triboelectric nanogenerator (FE-TENG). (a) The concept diagrams of the FE-TENG applied in river current. (b) Structure and materials of the FE-TENG. (c) Photographs of the FE-TENG and three different lengths of the bionic fins.

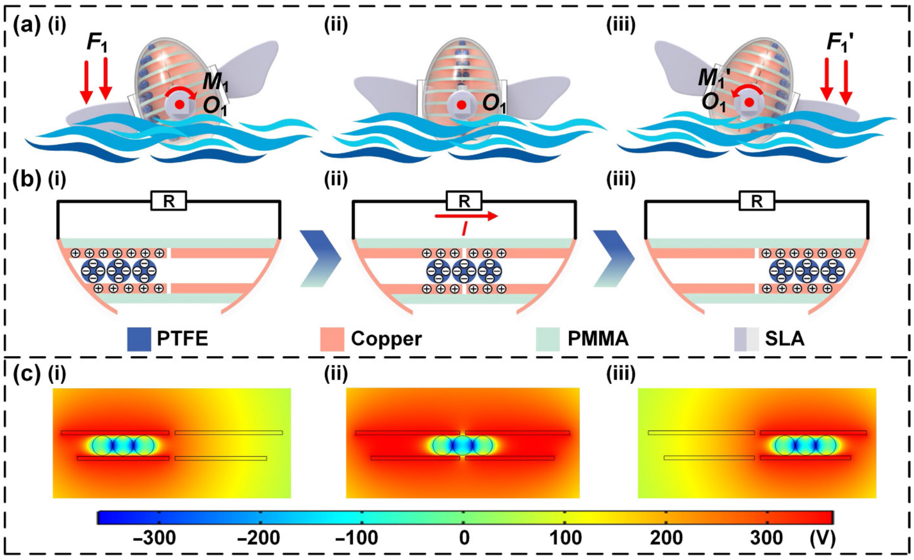

Figure 2 Operating principle of the FE-TENG: (a) Different operation states of the FE-TENG for half a cycle. (b) The working mechanism of the triboelectric power-generation unit. (c) Electrical potential distributions of the FE-TENG analyzed by COMSOL Multiphysics software.

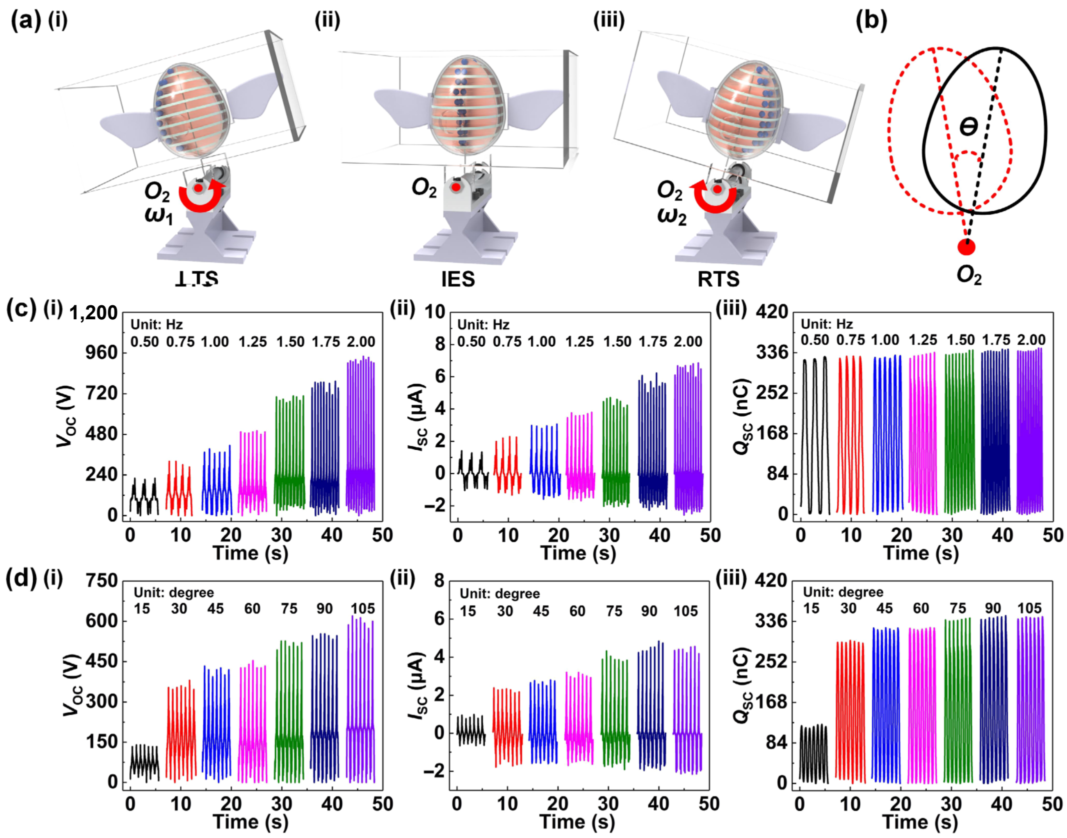

Figure 3 Electrical performance of the FE-TENG in the simulated swing state: (a) Working process of the left tilted state (LTS), the intermediate equilibrium state (IES), and the right tilted state (RTS) in a cycle and (b) swing angle of the FE-TENG. (c) Electrical performance of the FE-TENG by varying swing frequency from 0.50 to 2.00 Hz at swing angle of 60° and (d) ranging swing angle from 15° to 105° at frequency of 1.25 Hz.

the swing state of the FE-TENG in river current environment. The PTFE balls move from left to right on the copper electrodes as the swinging apparatus swing from the left tilted state (LTS) to the intermediate equilibrium state (IES) and then to the right tilted state (RTS). The swing angle, as indicated in Fig. 3(b), is kept at 60°, and the influence of frequency ranged from 0.50 Hz to 2.00 Hz on open-circuit voltage, short-circuit current and transferred charge of the FE-TENG is explored under the acceleration of 5 m/s^2, which is shown in Fig. 3(c). The transfer rate of negative electrons between the copper electrodes rises with the increasing of the swing frequency, resulting in increasing of short-circuit current from 1.4 to 6.8 μA (Fig. 3(c)(ii)), and the open-circuit voltage measured by a super phosphor oscilloscope varies from 220 to 940 V (Fig. 3(c)(i)). The transferred charge attained about 320 nC at 0.50 Hz and approximately remain stable as the PTFE balls and the copper electrodes have been almost fully contacted in the swing angle of 60° (Fig. 3(c)(iii)). The electrical performance of the device on swing angle ranged from 15° to 105° is further explored under the swing frequency of 1.25 Hz and acceleration of 5 m/s^2 (Fig. 3(d)). As the increasing of the swing angle implies that the effective contact area between the PTFE balls and the copper electrodes expands, all of the open-circuit voltage, short-circuit current and transferred charge display an increasing trend, and the electrical output of 520 V, 4.3 μA, and 340 nC are obtained at swing angle of 75° respectively. The electrical performance of the device with simulated translation state are depicted in Fig. S4 in the ESM. And Fig. S5 in the ESM shows the research on accelerations in the simulated translation state and swing state.

A water pump is used to power the simulated river current in a water tank to preferably explore the electrical performance of the FE-TENG. Since the flow velocity is unstable, the average flow velocities measured by a current meter are applied to represent the five flow states, and detailed information can be seen from Table S1 in the ESM. Figure 4 demonstrates the electrical performance of the device based on the relative position H representing the vertical distance from the horizontal center of the bionic fins to the O_1 at different flow velocities ranged from 0.21 to 0.81 m/s, and the length of bionic fins is 50 mm. The bionic fins are submerged in water at the relative position H_1 and H_2, and the device with relative position H_1 of the bionic fins has slightly lower electrical performance than H_2 as the later is closer to water surface that containes more hydrokinetic energy due to the wall effect, which are plotted in Figs. 4(a) and 4(b). The comparison between Figs. 4(b) and 4(c) shows that the device with relative position H_3 of the bionic fins partially immersed in water has higher electrical performance, especially at lower flow velocities such as 0.21 m/s, which proves that the device with high relative position of the bionic fins is conducive to harvest hydrokinetic energy of river current and benefit to realize zero head power generation in shallow water. But overhigh relative position of the bionic fins breaking out of the water is disadvantageous to be impacted by the river current. Increasing the flow velocity will enhance the impact force exerted to the bionic fins (Eq. (S1) in the ESM), resulting in a larger swing angle of the device with higher electrical performance. When the flow velocity is 0.81 m/s, the power generation potential of the device with relative positions H_3 of the bionic fins has been fully exploited with the approximate electrical output of 150 V, 1.3 μA and 140 nC. The detailed measurement results are shown in Fig. S6 in the ESM. Average output power of the device with relative positions H_3 of the bionic fins indicates the obvious advantage of electrical performance, which proves the rationality of the analyses (Fig. 4(d)). More than that, the device shows stable swing frequency ranged between 1.0 and 1.2 Hz at different flow velocities, indicating the capability to harvest hydrokinetic energy of river current at low flow velocity (Fig. 4(e)).

The electrical performance of the FE-TENG with the bionic fins at the length L_1 of 30 mm, L_2 of 50 mm and L_3 of 70 mm is measured respectively at different flow velocities ranged from 0.21 to 0.81 m/s, and relative position of the bionic fins is 15 mm, which is sketched in Fig. 5. When the device with bionic fins at length L_1, the potential electrical performance is laborious to be exploited (Fig. 5(a)). The longer bionic fins with larger bearing areas are taken a lot more impact force (Eq. (S1) in the ESM), demonstrating more prominent ability to harvest hydrokinetic energy of river current at lower flow velocities, such as 0.21 m/s, and the device with bionic fins at length L_2 and L_3 can generate the maximum electrical output of approximate 150 V, 1.3 μA and 140 nC (Figs. 5(b) and 5(c)). But the overlong bionic fins applied too much impact force are more likely to be damaged, and it would cause the uncoordinated swing of the device and affect the adaptability in the river current environment. The detailed measurement results are shown in Fig. S7 in the ESM. The device shows obvious advantages of electrical performance with bionic fins at length L_3 according to the average output power of the FE-TENG at different flow velocities as shown in Fig. 5(d). In addition, Fig. 5(e) shows steady swing frequency of the device ranged between 1.0 and 1.2 Hz, which indicates the adaptability for the low flow velocity. The results show that the device with bionic fish-like structure is capable to work at a low flow velocity continuously and realize potential applications to harvest hydrokinetic energy of river current.

2.3 Demonstration

The capacitors with capacitances ranged from 4.7 to 47.0 μF and a rectifier are used to investigate the charging capacity of the FE-TENG with swing angle of 75° and swing frequency of 1.25 Hz in 90 s, which is depicted in Fig. 6(a). The 4.7 μF capacitor is charged to 2 V in 13 s. With increasing of the capacitance, it takes more time to be charged to the same voltage, for example, 50 seconds is needed to charge a 22.0 μF capacitor to 2 V. In addition, the peak power density P_1 and P_2 under the simulated swing state and simulated river current environment are 7 and 0.36 W/m³ respectively with load resistance of 1,000 MΩ, as shown in Fig. 6(b). Furthermore, the device is immersed in water for 35 days without diminished electrical performance due to the 3D fully-enclosed design, demonstrating excellent immersion durability (Fig. 6(c)). The experimental platform based on the FE-TENG is installed to harvest hydrokinetic energy of river current, which can power a thermometer with the assistance of a 100 μF

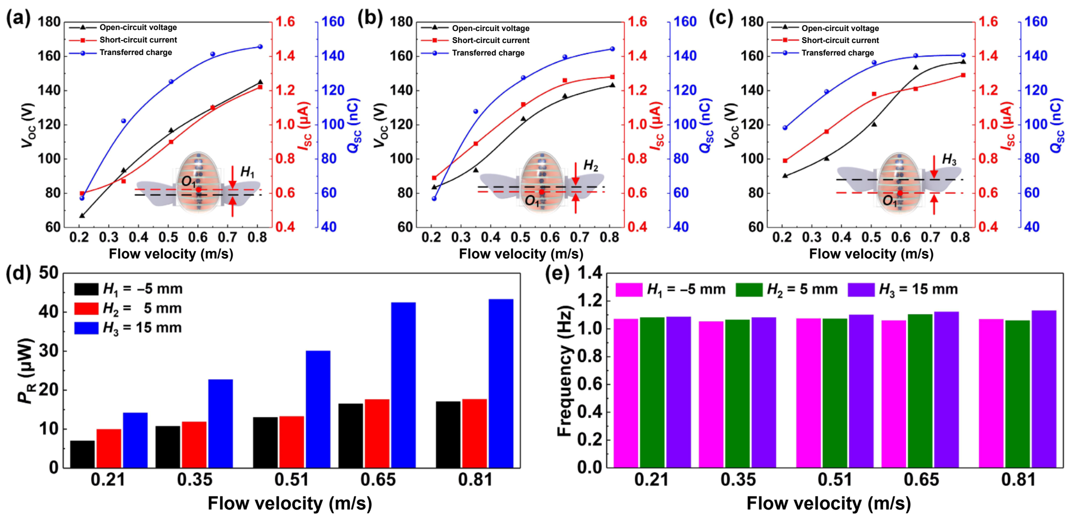

Figure 4 Research on the electrical performance of the FE-TENG with varying relative positions of the bionic fins. (a)–(c) Electrical performance of the FE-TENG with the bionic fins at relative position H_1 of -5 mm, H_2 of 5 mm and H_3 of 15 mm, respectively. (d) Average output power with load resistance of 1,000 MΩ and (e) swing frequency of the FE-TENG with varying relative positions of the bionic fins at different flow velocities.

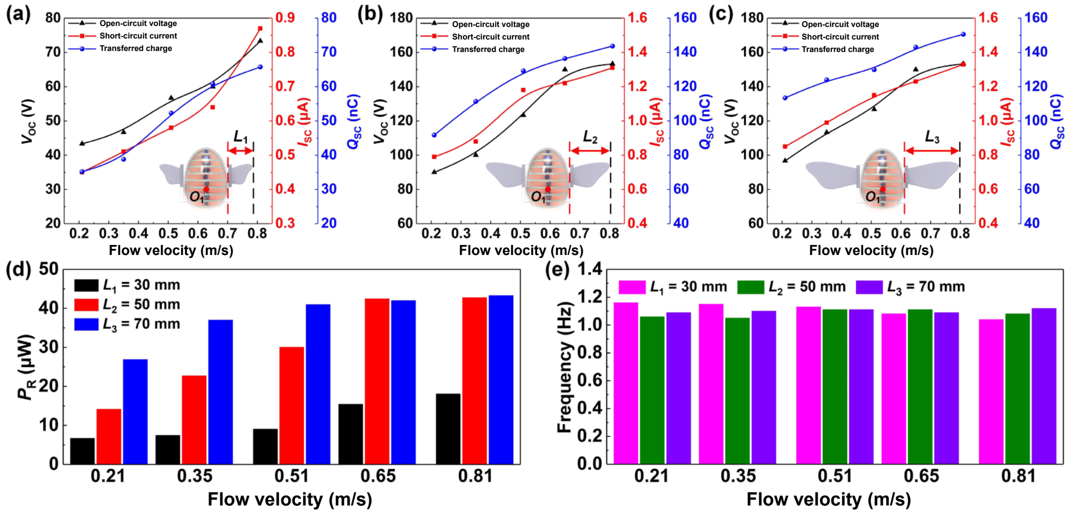

Figure 5 Research on the electrical performance of the FE-TENG with varying lengths of the bionic fins. (a)–(c) Electrical performance of the FE-TENG with the bionic fins at the length L_1 of 30 mm, L_2 of 50 mm and L_3 of 70 mm respectively. (d) Average output power with load resistance of 1,000 MΩ and (e) swing frequency of the FE-TENG with varying lengths of the bionic fins at different flow velocities.

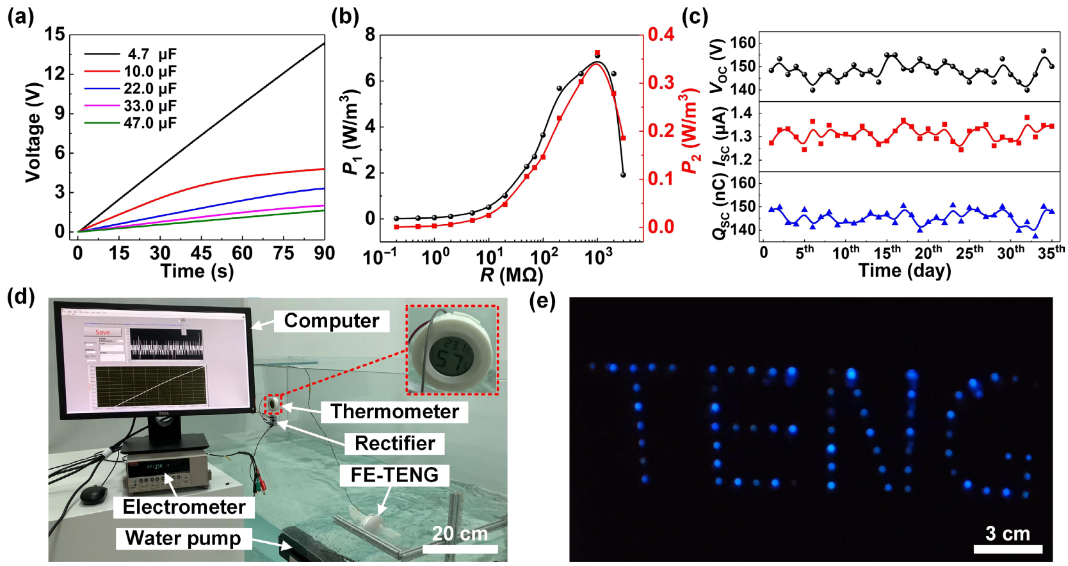

Figure 6 Electrical measurements and applications of the FE-TENG. (a) The capacitors ranged from 4.7 to 47.0 μF charged by the FE-TENG in 90 s. (b) Electrical performance of power density with load resistances ranged from 0.2 to 3,000 MΩ. (c) Water immersion durability of the device within 35 days. (d) A thermometer or (e) 67 LEDs powered by the FE-TENG.

capacitor (Fig. 6(d) and Movie ESM1) and illumine 67 light-emitting diodes (LEDs) in series through the rectifier (Fig. 6(e) and Movie ESM2) under the simulated river current environment. Therefore, the FE-TENG provides a potential approach for long-term service in river current to harvest hydrokinetic energy and provide power supply for electronic devices.

3 Conclusions

In summary, a 3D fully-enclosed triboelectric nanogenerator (FE-TENG) with bionic fish-like structure is proposed to convert hydrokinetic energy of river current to electrical output. It consists of the triboelectric power-generation unit, bionic fish-like structure and connection unit. The device realizes zero head power generation in shallow water with low flow velocity due to the bionic fish-like structure. In addition, the effects of external excitations on the electrical performances are also investigated from both experimental and theoretical aspects. The experiment results show the FE-TENG can generate output of 520 V, 4.3 μA, 340 nC and peak power density of 7 W/m³ under the simulated swing state with frequency of 1.25 Hz. To explore the performance under practical river current environment, the output of 150 V, 1.3 μA, 140 nC and peak power density of 0.36 W/m³ is generated under the excitation of simulated river current with flow velocity of 0.81 m/s. What's more, the FE-TENG immersed in water for 35 days without diminished electrical performance due to the 3D fully-enclosed design, which indicates the excellent water immersion durability and demonstrates the great potencial capacity for long-term service in the river current. Therefore, it has the potential to open up new applications in remote regions and other difficult-to-access locations where batteries and conventional power are unrealistic.

4 Experimental section

4.1 Fabrication of the FE-TENG

The 3D fully-enclosed triboelectric nanogenerator (FE-TENG) device is composed of a bionic shell, a pair of bionic fins, PTFE balls, copper electrodes, substrates, and connection unit. The connection unit consists of two connectors at both ends and a spring held in the middle. In addition, the bionic shell has dimensions of 135 mm (length) × 80 mm (height) × 60 mm (width), and it is 3D printed with a thickness of 2 mm. In order to explore the influence of the bionic structure on electrical performance, three specifications of the bionic fins are designed with the lengths of 30, 50, and 70 mm, respectively. The copper electrodes with thickness of 50 μm are attached onto two sides of the substrates cut from PMMA sheets with thickness of 3 mm. The PTFE balls with a mass of 38 g and a diameter of 5 mm move freely on the surface of the copper electrodes. Additional information are presented in Electronic Supplementary Material.

4.2 Electrical measurement

A linear motor (LinMot PL01-19 × 600/520) and a water pump (SCP-180, Jiebao, China) provide the power supply for the movement of the FE-TENG. A programmable electrometer (6514, Keithley, USA) and a data acquisition system (USB-6218, National Instruments, USA) are employed for measuring the short-circuit current and the transferred charge, and a super phosphor oscilloscope (SDS2204X, Siglent, China) is used to measuring the open-circuit voltage. The flow velocities are measured by a current meter (LS300-A, Zhuoma, China).

Acknowledgements

The authors are grateful for the support received from the National Key R&D Project from the Minister of Science and Technology (Nos. 2021YFA1201601 and 2021YFA1201604), and the Natural Science Foundation of Beijing Municipality (No. 3222023)).

Conflict of interest

The authors declare no conflict of interest.

Electronic Supplementary Material: Supplementary material (additional figures and movies, including the operating principle and mechanical analysis of the FE-TENG, the finite element simulation of pressure field distribution of the FE-TENG with varying lengths and different relative positions of the bionic fins, electrical performance of the FE-TENG under different external excitations, detailed numerical value of flow velocities and demonstration movies of powering the electronic devices by the FE-TENG) is available in the online version of this article at https://doi.org/10.1007/s12274-022-4131-y.

References

[1] Wang, Z. L.; Song, J. H. Piezoelectric nanogenerators based on zinc oxide nanowire arrays. *Science* **2006**, *312*, 242–246.

[2] Wang, Z. L. Entropy theory of distributed energy for internet of things. *Nano Energy* **2019**, *58*, 669–672.

[3] Wang, Z. L. Triboelectric nanogenerators as new energy technology and self-powered sensors-principles, problems and perspectives. *Faraday Discuss.* **2014**, *176*, 447–458.

[4] Yang, Z. B.; Zhou, S. X.; Zu, J.; Inman, D. High-performance piezoelectric energy harvesters and their applications. *Joule* **2018**, *2*, 642–697.

[5] New, T.; Xie, Z. Q. Impacts of large dams on riparian vegetation: Applying global experience to the case of China' s Three Gorges Dam. *Biodivers. Conserv.* **2008**, *17*, 3149–3163.

[6] Maavara, T.; Chen, Q. W.; Van Meter, K.; Brown, L. E.; Zhang, J. Y.; Ni, J. R.; Zarfl, C. River dam impacts on biogeochemical cycling. *Nat. Rev. Earth Environ.* **2020**, *1*, 103–116.

[7] Zi, Y. L.; Guo, H. Y.; Wen, Z.; Yeh, M. H.; Hu, C. G.; Wang, Z. L. Harvesting low-frequency (<5 Hz) irregular mechanical energy: A possible killer application of triboelectric nanogenerator. *ACS Nano* **2016**, *10*, 4797–4805.

[8] Zhang, C.; Tang, W.; Han, C. B.; Fan, F. R.; Wang, Z. L. Theoretical comparison, equivalent transformation, and conjunction operations of electromagnetic induction generator and triboelectric nanogenerator for harvesting mechanical energy. *Adv. Mater.* **2014**, *26*, 3580–3591.

[9] Wang, Z. L. On the first principle theory of nanogenerators from Maxwell's equations. *Nano Energy* **2020**, *68*, 104272.

[10] Wang, Z. L. Nanogenerators, self-powered systems, blue energy, piezotronics and piezo-phototronics - a recall on the original thoughts for coining these fields. *Nano Energy* **2018**, *54*, 477–483.

[11] Wang, Z. L. On Maxwell's displacement current for energy and sensors: The origin of nanogenerators. *Mater. Today* **2017**, *20*, 74–82.

[12] Fan, F. R.; Tian, Z. Q.; Wang, Z. L. Flexible triboelectric generator. *Nano Energy* **2012**, *1*, 328–334.

[13] Lin, L.; Xie, Y. N.; Niu, S. M.; Wang, S. H.; Yang, P. K.; Wang, Z. L. Robust triboelectric nanogenerator based on rolling electrification and electrostatic induction at an instantaneous energy conversion efficiency of ~55%. *Acs Nano* **2015**, *9*, 922–930.

[14] Wu, C. S.; Wang, A. C.; Ding, W. B.; Guo, H. Y.; Wang, Z. L. Triboelectric nanogenerator: A foundation of the energy for the new era. *Adv. Energy Mater.* **2019**, *9*, 1802906.

[15] Wang, Z. L.; Chen, J.; Lin, L. Progress in triboelectric nanogenerators as a new energy technology and self-powered sensors. *Energy Environ. Sci.* **2015**, *8*, 2250–2282.

[16] Wang, Z. L. From contact electrification to triboelectric nanogenerators. *Rep. Prog. Phys.* **2021**, *84*, 096502.

[17] Chen, J.; Yang, J.; Guo, H. Y.; Li, Z. L.; Zheng, L.; Su, Y. J.; Wen, Z.; Fan, X.; Wang, Z. L. Automatic mode transition enabled robust triboelectric nanogenerators. *ACS Nano* **2015**, *9*, 12334–12343.

[18] Wang, Z. L.; Wu, W. Z. Nanotechnology-enabled energy harvesting for self-powered micro-/nanosystems. *Angew. Chem., Int. Ed.* **2012**, *51*, 11700–11721.

[19] Wang, Z. L. Triboelectric nanogenerators as new energy technology for self-powered systems and as active mechanical and chemical sensors. *ACS Nano* **2013**, *7*, 9533–9557.

[20] Wang, J. L.; Li, Y. K.; Xie, Z. J.; Xu, Y. H.; Zhou, J. W.; Cheng, T. H.; Zhao, H. W.; Wang, Z. L. Cylindrical direct-current triboelectric nanogenerator with constant output current. *Adv. Energy Mater.* **2020**, *10*, 1904227.

[21] Jing, Q. S.; Zhu, G.; Bai, P.; Xie, Y. N.; Chen, J.; Han, R. P. S.; Wang, Z. L. Case-encapsulated triboelectric nanogenerator for harvesting energy from reciprocating sliding motion. *ACS Nano* **2014**, *8*, 3836–3842.

[22] Wang, Z.; Yu, Y.; Wang, Y. T.; Lu, X. H.; Cheng, T. H.; Bao, G.; Wang, Z. L. Magnetic flap-type difunctional sensor for detecting pneumatic flow and liquid level based on triboelectric nanogenerator. *ACS Nano* **2020**, *14*, 5981–5987.

[23] Gao, Q.; Cheng, T. H.; Wang, Z. L. Triboelectric mechanical sensors - progress and prospects. *Extreme Mech. Lett.* **2021**, *42*, 101100.

[24] Chen, J.; Wang, Z. L. Reviving vibration energy harvesting and self-powered sensing by a triboelectric nanogenerator. *Joule* **2017**, *1*, 480–521.

[25] Zhao, X.; Askari, H.; Chen, J. Nanogenerators for smart cities in the era of 5G and internet of things. *Joule* **2021**, *5*, 1391–1431.

[26] Jin, L.; Deng, W. L.; Su, Y. C.; Xu, Z.; Meng, H.; Wang, B.; Zhang, H. P.; Zhang, B. B.; Zhang, L.; Xiao, X. B. et al. Self-powered wireless smart sensor based on maglev porous nanogenerator for train monitoring system. *Nano Energy* **2017**, *38*, 185–192.

[27] Jin, L.; Zhang, S. L.; Xu, S. X.; Guo, H. Y.; Yang, W. Q.; Wang, Z. L. Free-fixed rotational triboelectric nanogenerator for self-powered real-time wheel monitoring. *Adv. Mater. Technol.* **2021**, *6*, 2000918.

[28] Wang, Z. L.; Jiang, T.; Xu, L. Toward the blue energy dream by triboelectric nanogenerator networks. *Nano Energy* **2017**, *39*, 9–23.

[29] Wang, Z. L. Catch wave power in floating nets. *Nature* **2017**, *542*, 159–160.

[30] Tang, W.; Chen, B. D.; Wang, Z. L. Recent progress in power generation from water/liquid droplet interaction with solid surfaces. *Adv. Funct. Mater.* **2019**, *29*, 1901069.

[31] Chen, J.; Yang, J.; Li, Z. L.; Fan, X.; Zi, Y. L.; Jing, Q. S.; Guo, H. Y.; Wen, Z.; Pradel, K. C.; Niu, S. M. et al. Networks of triboelectric nanogenerators for harvesting water wave energy: A potential approach toward blue energy. *ACS Nano* **2015**, *9*, 3324–3331.

[32] Wang, Z. L. Triboelectric nanogenerator (TENG)-sparking an energy and sensor revolution. *Adv. Energy Mater.* **2020**, *10*, 2000137.
[33] Lei, R.; Shi, Y. X.; Ding, Y. F.; Nie, J. H.; Li, S. Y.; Wang, F.; Zhai, H.; Chen, X. Y.; Wang, Z. L. Sustainable high-voltage source based on triboelectric nanogenerator with a charge accumulation strategy. *Energy Environ. Sci.* **2020**, *13*, 2178–2190.
[34] Guo, H. Y.; Chen, J.; Wang, L. F.; Wang, A. C.; Li, Y. F.; An, C. H.; He, J. H.; Hu, C. G.; Hsiao, V. K. S.; Wang, Z. L. A highly efficient triboelectric negative air ion generator. *Nat. Sustain.* **2021**, *4*, 147–153.
[35] Liang, X.; Jiang, T.; Liu, G. X.; Feng, Y. W.; Zhang, C.; Wang, Z. L. Spherical triboelectric nanogenerator integrated with power management module for harvesting multidirectional water wave energy. *Energy Environ. Sci.* **2020**, *13*, 277–285.
[36] Yang, X. D.; Xu, L.; Lin, P.; Zhong, W.; Bai, Y.; Luo, J. J.; Chen, J.; Wang, Z. L. Macroscopic self-assembly network of encapsulated high-performance triboelectric nanogenerators for water wave energy harvesting. *Nano Energy* **2019**, *60*, 404–412.
[37] Yin, M. F.; Lu, X. H.; Qiao, G. D.; Xu, Y. H.; Wang, Y. Q.; Cheng, T. H.; Wang, Z. L. Mechanical regulation triboelectric nanogenerator with controllable output performance for random energy harvesting. *Adv. Energy Mater.* **2020**, *10*, 2000627.
[38] Xu, L.; Jiang, T.; Lin, P.; Shao, J. J.; He, C.; Zhong, W.; Chen, X. Y.; Wang, Z. L. Coupled triboelectric nanogenerator networks for efficient water wave energy harvesting. *ACS Nano* **2018**, *12*, 1849–1858.
[39] Zhang, C. G.; He, L. X.; Zhou, L. L.; Yang, O.; Yuan, W.; Wei, X. L.; Liu, Y. B.; Lu, L.; Wang, J.; Wang, Z. L. Active resonance triboelectric nanogenerator for harvesting omnidirectional water-wave energy. *Joule* **2021**, *5*, 1613–1623.
[40] Zhu, G.; Su, Y. J.; Bai, P.; Chen, J.; Jing, Q. S.; Yang, W. Q.; Wang, Z. L. Harvesting water wave energy by asymmetric screening of electrostatic charges on a nanostructured hydrophobic thin-film surface. *ACS Nano* **2014**, *8*, 6031–6037.
[41] Su, Y. J.; Wen, X. N.; Zhu, G.; Yang, J.; Chen, J.; Bai, P.; Wu, Z. M.; Jiang, Y. D.; Wang, Z. L. Hybrid triboelectric nanogenerator for harvesting water wave energy and as a self-powered distress signal emitter. *Nano Energy* **2014**, *9*, 186–195.
[42] Zhou, H.; Li, D. X.; He, X. M.; Hui, X. D.; Guo, H. Y.; Hu, C. G.; Mu, X. J.; Wang, Z. L. Bionic ultra-sensitive self-powered electromechanical sensor for muscle-triggered communication application. *Adv. Sci.* **2021**, *8*, 2101020.
[43] Yang, J.; Chen, J.; Su, Y. J.; Jing, Q. S.; Li, Z. L.; Yi, F.; Wen, X. N.; Wang, Z. N.; Wang, Z. L. Eardrum-inspired active sensors for self-powered cardiovascular system characterization and throat-attached anti-interference voice recognition. *Adv. Mater.* **2015**, *27*, 1316–1326.
[44] Chen, B. D.; Tang, W.; He, C.; Deng, C. R.; Yang, L. J.; Zhu, L. P.; Chen, J.; Shao, J. J.; Liu, L.; Wang, Z. L. Water wave energy harvesting and self-powered liquid-surface fluctuation sensing based on bionic-jellyfish triboelectric nanogenerator. *Mater. Today* **2018**, *21*, 88–97.
[45] Bu, T. Z.; Xiao, T. X.; Yang, Z. W.; Liu, G. X.; Fu, X. P.; Nie, J. H.; Guo, T.; Pang, Y. K.; Zhao, J. Q.; Xi, F. B. et al. Stretchable triboelectric-photonic smart skin for tactile and gesture sensing. *Adv. Mater.* **2018**, *30*, 1800066.
[46] Feilich, K. L. Correlated evolution of body and fin morphology in the cichlid fishes. *Evolution* **2016**, *70*, 2247–2267.
[47] Wang, Z. L.; Wang, A. C. On the origin of contact-electrification. *Mater. Today* **2019**, *30*, 34–51.
[48] Niu, S. M.; Wang, Z. L. Theoretical systems of triboelectric nanogenerators. *Nano Energy* **2015**, *14*, 161–192.